TU Delft

Delft University of Technology

Document Version
Final published version

Licence
CC BY

Citation (APA)
Haaf, S. L. D. T., Miles, S., Wang, Q., Bozkurt, A. M., Kulesh, I., Zhang, Y., Prosko, C. G., Wimmer, M., & Goswami, S. (2026). Probing Ground-State Degeneracies of a Strongly Interacting Fermi-Hubbard Model with Superconducting Correlations. *Physical review letters*, *137*(12), Article 126503. https://doi.org/10.1103/nz6v-xxrv

Important note
To cite this publication, please use the final published version (if applicable).
Please check the document version above.

Copyright
In case the licence states “Dutch Copyright Act (Article 25fa)”, this publication was made available Green Open Access via the TU Delft Institutional Repository pursuant to Dutch Copyright Act (Article 25fa, the Taverne amendment). This provision does not affect copyright ownership.
Unless copyright is transferred by contract or statute, it remains with the copyright holder.

Sharing and reuse
Other than for strictly personal use, it is not permitted to download, forward or distribute the text or part of it, without the consent of the author(s) and/or copyright holder(s), unless the work is under an open content license such as Creative Commons.

Takedown policy
Please contact us and provide details if you believe this document breaches copyrights.
We will remove access to the work immediately and investigate your claim.

This work is downloaded from Delft University of Technology.

Probing Ground-State Degeneracies of a Strongly Interacting Fermi-Hubbard Model with Superconducting Correlations

Sebastiaan L. D. ten Haaf,* Sebastian Miles,* Qingzhen Wang, A. Mert Bozkurt, Ivan Kulesh, Yining Zhang, Christian G. Prosko, Michael Wimmer, and Srijit Goswami†

QuTech and Kavli Institute of Nanoscience, Delft University of Technology, Delft, 2600 GA, The Netherlands

(Received 15 December 2025; accepted 16 July 2026; published 15 September 2026)

The Fermi-Hubbard model describes a large variety of condensed matter systems with spinful fermions and strong interactions. On the other hand, the Kitaev chain model deals with noninteracting spinless fermions and produces robust ground-state degeneracies that give rise to Majorana bound states. In this Letter, we connect these two domains by experimentally studying small arrays of quantum dots (QDs) coupled via superconductors. Without a magnetic field, this system constitutes a Fermi-Hubbard model with intersite superconducting correlations. Using two coupled QDs, we find sweet spots in parameter space where we observe zero-bias conductance peaks that are robust against on-site perturbations of the QDs, similar to the behavior expected of a two-site Kitaev chain. This observation is consistent with the presence of Majorana Kramers pairs or $\mathbb{Z}_3$ parafermions in this minimal system. Extending to three sites, we find that the spinful system scales very differently compared to the spinless Kitaev chain. When the same sweet-spot conditions are satisfied, the ground state degeneracy of the full three-site system is lifted. The degeneracy can be restored by tuning the superconducting phase difference between the hybrid segments, but the robustness against on-site detunings is lost. Our findings are a first step in studying ground-state degeneracies in strongly interacting Fermi-Hubbard systems with superconducting correlations.

DOI: 10.1103/nz6v-xxrv

Introduction—The Fermi-Hubbard model is a fundamental model for strongly correlated electron systems, capturing the competition between electron kinetic energy and on-site Coulomb repulsion [1,2]. Despite its seeming simplicity, the model exhibits a rich phase diagram [2,3]. This fundamental importance has motivated experimental efforts to realize the Fermi-Hubbard model in controllable platforms such as ultracold atoms [4], trapped ions [5], and superconducting circuits [6,7]. Semiconductor quantum dots are another natural platform, due to intrinsic strong electron-electron interactions from on-site Coulomb repulsion [8]. Recent experiments have studied different aspects of the Fermi-Hubbard model using small quantum dot arrays [9,10].

Semiconductor quantum dots were also put forth as a platform for a noninteracting model exhibiting topological superconductivity—the Kitaev chain [11–14]. Recently, short Kitaev chains were successfully implemented using small arrays of quantum dots coupled by superconducting hybrid segments [15–18]. In addition to normal electron hopping between quantum dots, the superconducting segments mediate Cooper pair splitting, effectively implementing a p-wave pairing between neighboring quantum dots [19,20]. Though the charging energy is the largest energy scale in these devices [16], the effects of interactions are minimized by a Zeeman splitting on the QDs, effectively suppressing interactions between different spin species.

In this work, we combine these two research directions, and study a superconducting extension of the Fermi-Hubbard model using quantum dot arrays. We experimentally implement short chains of quantum dots coupled by superconducting hybrid segments, as used to implement Kitaev chains [15,16,21], but in the absence of a magnetic field. In this regime, the effect of electron interactions is restored. This effectively yields a one-dimensional Fermi-Hubbard model with an additional nearest-neighbor, spatially odd pairing term. This model was recently shown theoretically to feature peculiar ground state degeneracies due to the interplay of strong interactions and superconducting pairing [22]. In particular, the two-site system was predicted to exhibit a threefold degenerate spectrum [22] where strong $\mathbb{Z}_3$ zero modes emerge [23,24].

We implement devices with two and three interacting sites on InSbAs 2DEGs with epitaxial Al and study their

*These authors contributed equally to this work.
†Contact author: s.goswami@tudelft.nl

Published by the American Physical Society under the terms of the Creative Commons Attribution 4.0 International license. Further distribution of this work must maintain attribution to the author(s) and the published article's title, journal citation, and DOI.

low energy conductance spectra. Our experiments reproduce the main theoretical predictions in Ref. [22]: a stable ground state degeneracy is observed in the two-site chains, which is lifted when adding a third site. Additionally, we find in both theory and experiment that introducing a superconducting phase difference allows to fine-tune also the three-site system to a strongly degenerate configuration. The striking agreement between experiment and theory suggests that the quantum dot platform is well suited to explore the interplay of strong correlations and superconductivity in extended Fermi-Hubbard type models.

The spinful QD chain model—A chain of QDs coupled via superconductors can be described by a Fermi-Hubbard Hamiltonian with an additional nearest-neighbor superconducting term:

$$H = H_{\mathrm{D}} + H_{\mathrm{U}} + H_{\mathrm{ECT}} + H_{\mathrm{CAR}}. \tag{1}$$

Here, $H_{\mathrm{D}} = \sum_i \mu_i (n_{i,\uparrow} + n_{i,\downarrow})$ models the QDs chemical potential μ_i, while $H_{\mathrm{U}} = \sum_i U_i n_{i,\uparrow} n_{i,\downarrow}$ models the on-site Coulomb repulsion. The superconducting segment hosts gate-tunable Andreev bound states that generate two virtual transport processes coupling the neighboring QDs [19,25–28]. Elastic cotunneling (ECT) facilitates hopping of an electron between two neighboring sites. We model this process as $H_{\mathrm{ECT}} = \sum_i t^{(i,i+1)} (c^\dagger_{i,\uparrow} c_{i+1,\uparrow} + c^\dagger_{i,\downarrow} c_{i+1,\downarrow}) + \mathrm{H.c.}$. Crossed Andreev reflection (CAR), modeled by $H_{\mathrm{CAR}} = \sum_i \Delta^{(i,i+1)} (c^\dagger_{i,\uparrow} c^\dagger_{i+1,\downarrow} - c^\dagger_{i,\downarrow} c^\dagger_{i+1,\uparrow}) + \mathrm{H.c.}$, facilitates an s-wave pairing interaction via the creation or breaking of Cooper pairs.

In our devices the typical interdot coupling is on the order of 20 μV, while typical charging energies are on the order of 1–2 mV, making Coulomb repulsion the largest energy scale (Fig. S1 [29]). We therefore consider the limit $U = \infty$ for comparing experiments and theory. To capture this, we project out the double occupancy restricting us to an effective basis $\{|0\rangle, |\uparrow\rangle, |\downarrow\rangle\}$ on each QD. For two QD sites a sweet spot is expected at $\mu_1 = \mu_2 = 0$ and $t^{(1,2)} = \sqrt{2}\Delta^{(1,2)}$ [30,31], where the ground state of the system is threefold degenerate and hosts Majorana Kramers pairs [22], which are stable against detuning of individual QDs. Experimentally, we start by characterizing such sweet spots in a two QD system and study the evolution of the low-energy spectrum when adding a third QD.

Device and measurement setup—The device studied in the main text is shown in Fig. 1(b), containing three quantum dots and two superconducting regions. The two SC strips (green) are connected in a loop and kept grounded. An external magnetic field B_z controls the superconducting phase difference between the strips. Andreev bound states (ABSs) are induced in the regions proximitized by the SCs (Fig. S1 [29]). The energies of the ABSs in the left and right hybrid sections are controlled by the voltages $V^{(1)}_{\mathrm{ABS}}$ and $V^{(2)}_{\mathrm{ABS}}$. Three large gates (red) confine

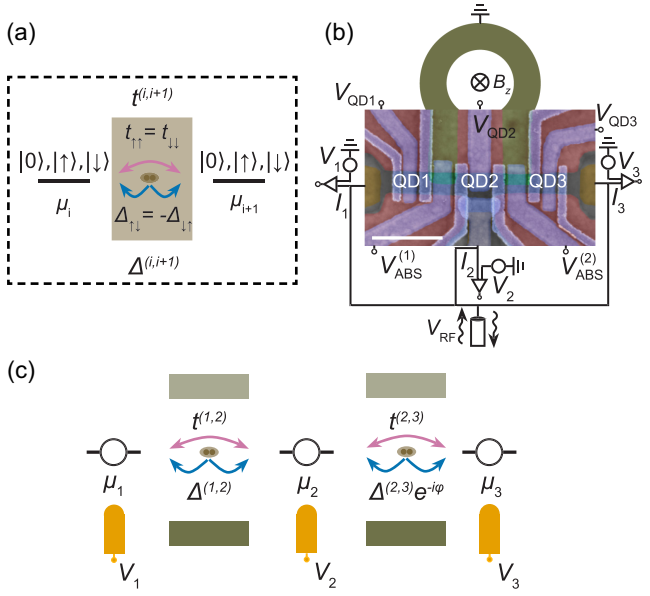


FIG. 1. Model and device schematics (a) Schematic of the nearest-neighbor interactions for two spinful fermionic sites coupled via a superconductor. We assume here $t^{(i,j)} = t^{(i,j)}_{\downarrow\downarrow} = t^{(i,j)}_{\uparrow\uparrow}$ and $\Delta^{(i,j)} = \Delta^{(i,j)}_{\uparrow\downarrow} = -\Delta^{(i,j)}_{\downarrow\uparrow}$ (sign due to time reversal symmetry). In the $U \to \infty$ limit, the doubly occupied state is disallowed. (b) False color scanning electron micrograph of a copy of device A. Two aluminium strips are connected via a continuous loop with a radius of 10 μm (not drawn to scale). Scale bar is 500 nm. (c) Schematic representation of the device, highlighting relevant the parameters for theoretical simulations.

a quasi-1D channel. Narrow finger gates (blue) confine three QDs and control their electrochemical potentials (V_{QDi}). Each QD is probed by an ohmic lead, to record the device conductance in two separate ways. Applied voltages (V_1, V_2, and V_3) and measured currents (I_1, I_2 and I_3) are used to measure the local differential conductance in each lead [$G_{ii} = (dI_i/dV_i)$]. In addition, off-chip resonators allow for measuring the RF-reflectometry response, denoted $\tilde{S}_{\mathrm{i}}$ (for details, see Methods and Fig. S2) [29]. This signal is linearly proportional to the device conductance in the regime of interest [32–35].

Results—

The two-site chain: After forming three QDs through electrostatic tuning, we first focus on the coupling between QD1 and QD2, keeping QD3 off-resonance. In this two-site system, the simultaneous presence of ECT and CAR creates a competition between different parity ground-states [13,15,16,20,21]. ECT couples states with the same total particle number, whereas CAR couples states whose particle number differs by 2. Notably, this competition exists also without an external magnetic field [36]. To study this, we measure charge stability diagrams (CSDs) across a single orbital in each QD. When ECT dominates, diagonal avoided crossings are expected, as shown in an exemplary measurement in Fig. 2(a). Control over $V^{(1)}_{\mathrm{ABS}}$ affects the

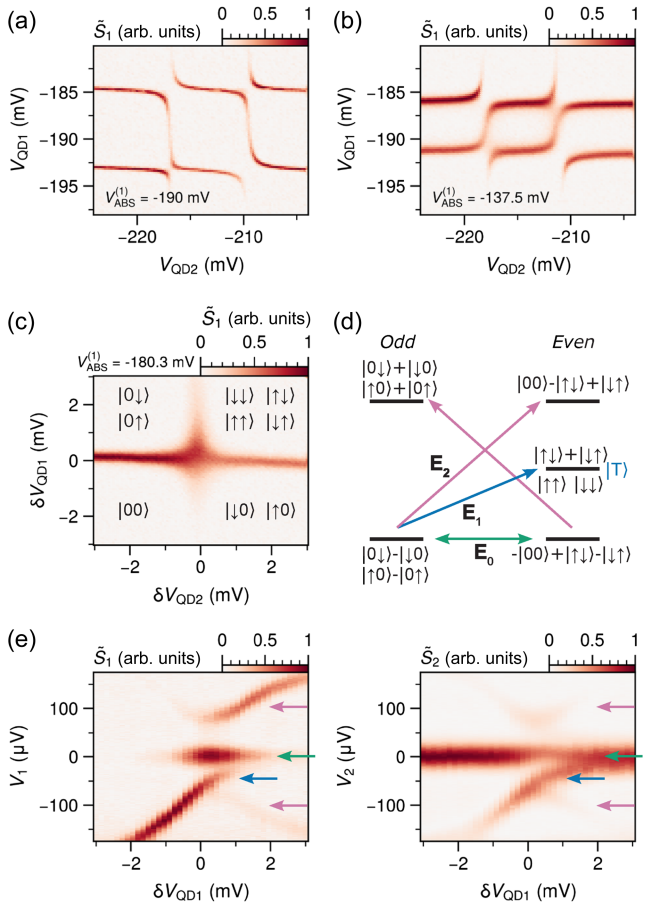


FIG. 2. The two-site sweet spot. Tuning the coupling between QD1 and QD2, with QD3 tuned to a Coulomb blockaded regime. (a) Exemplar CSD in an ECT dominated regime [$V^{(1)}_{\mathrm{ABS}} = -190$ mV], showing four anti-diagonal avoided crossings. (b) Exemplar CSD in a CAR dominated regime [$V^{(1)}_{\mathrm{ABS}} = -137.5$ mV], showing four diagonal avoided crossings. Examples were chosen to showcase the change in connectivity can arise in all 4 quadrants of the CSDs. More general CSDs are shown in Fig. S3. (c) Close up CSD of the bottom left quadrant, at an intermediate value of $V^{(1)}_{\mathrm{ABS}} = -180.3$ mV. (d) Energy level diagram for the two parity sectors at the sweet spot. Coherence factors have been omitted. (e) Tunnelling spectroscopy measured when detuning V_{QD1}, with V_{QD2} set on resonance. Colored arrows correspond to transitions indicated in (d). Reproduction of results in a separate device is shown in Figs. S5–S7.

underlying CAR and ECT processes, changing the CSD. Moving $V^{(1)}_{\mathrm{ABS}}$ by ≈50 mV, the CSD now only shows antidiagonal avoided crossings [Fig. 2(b)], indicating CAR has become the dominant process. This continuous control ensures that, for each pair of resonances, a "sweet-spot" exists where the avoided crossing disappears. There, zero-energy modes are expected to arise that are resilient against detuning individual QDs and protected to at least second-order against detuning both QDs [22]. Zooming in on the bottom-left pair of transitions and fine-tuning $V^{(1)}_{\mathrm{ABS}}$, we find such a sweet spot in Fig. 2(c).

To understand the density of states, we consider the energy level diagram of the effective model at the sweet spot ($t^{(1,2)} = \sqrt{2}\Delta^{(1,2)}$, $\mu_{\mathrm{i}} = 0$) in Fig. 2(d). The spectrum is strongly degenerate, meaning all energy manifolds feature a threefold degeneracy. This allows for single-electron transitions from the ground states at three possible energies, labeled by the colored arrows. We measure these transitions through lead reflectometry of lead 1 and lead 2, while sweeping V_{QD1}, where the expected transitions can be clearly identified [Fig. 2(e)]. Most trivially, we observe excitations which disperse with V_{QD1}, denoted as E_2 (pink). Second, we find a transition appearing only at negative bias (blue). This transition, denoted E_1, is a signature of the presence of the triplet states (denoted $|\mathrm{T}\rangle$) in the even parity subspace [36], breaking particle hole symmetry in the conductance spectrum. Lastly, we find zero-bias conductance peaks (green) that persist when detuning V_{QD1}. This reflects the zero-energy excitations (E_0) between the degenerate even and odd ground-states. The observed energy level structure is consistent with the zero-field limit of the magnetic-field evolution reported in [16], where the excitation spectrum was tracked continuously as time-reversal symmetry was broken. The many-body interpretation presented here now allows us to identify the zero-field degenerate ground-state excitations as arising from Kramers pairs of Majorana modes, or more exotically as $\mathbb{Z}_3$ parafermions, as detailed in [22]. Unlike Majoranas in the Kitaev chain, these are many-body excitations and therefore not localized on either QD [22]. Such localized Majorana modes emerge in the same system only once a magnetic field lifts the Kramers degeneracy [16]. Nevertheless, they are robust against perturbing the chemical potential of either of the QDs (see Fig. S4).

Scaling from two to three sites: At finite magnetic fields, the conditions giving rise to stable zero modes in the two-site chain could be extended to obtain stable zero modes in longer chains [12]. By satisfying the sweet spot condition between all pairs of neighboring QDs and setting all QDs on resonance, stable ZBPs are expected on the outermost sites, which was recently demonstrated [17,18]. As shown in [37], this is not possible generally. A crucial aspect of the strong degeneracy in our two-site system is that the triplet states [denoted $|T\rangle$ in Fig. 2(d)] decouple from the rest of the system [22]. This breaks down when turning on the coupling to a third site, even when tuning $t^{(2,3)}, \Delta^{(2,3)}$ to a sweet spot. To demonstrate this, we first repeat the procedure in Fig. 2 for QD2 and QD3, with QD1 off resonance, to obtain a $t^{(2,3)} = \sqrt{2}\Delta^{(2,3)}$ sweet spot (Fig. S4 [29]). With either of the outer QDs off resonance, the remaining two QDs then host stable ZBPs. Next, we bring all three QDs on resonance and perform finite-bias spectroscopy measurements. Figure 3(a) shows RF-spectroscopy measurements of $\tilde{S}_1$ and $\tilde{S}_3$, when detuning V_{QD3}. We observe that the ZBPs now split in energy as soon as δV_{QD3} approaches resonance. This is in stark

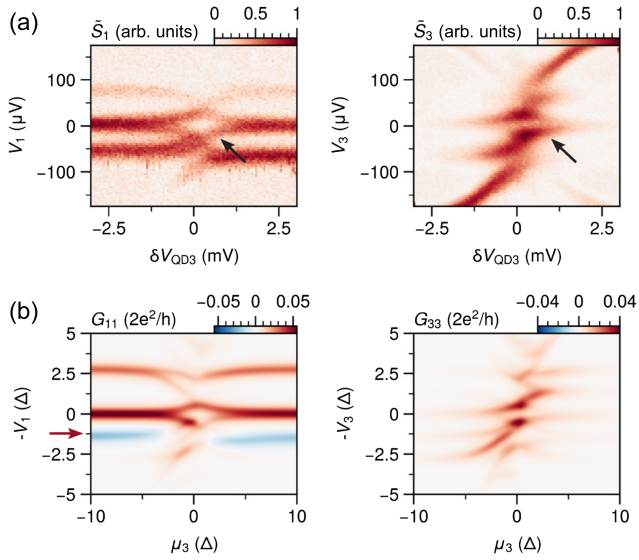


FIG. 3. Scaling from two to three sites. Measurements obtained with both pairs of QDs tuned to a sweet spot configuration. (a) Spectroscopy of the left ($\tilde{S}_1$) and right ($\tilde{S}_3$) side of the device while sweeping V_{QD3}. Once QD3 is on resonance, the ZBP on both sides is observed to split, indicated by the black arrows. (b) Numerically calculated conductance for varying μ_3, with $\mu_1 = \mu_2 = 0$ and $t = \sqrt{2}\Delta$. A similar behavior is observed: the ground-state degeneracy is lifted as μ_3 approached 0. An interesting feature in the numerics is the negative local conductance of the excited state marked by the red arrow. This arises from a dynamical blockade related to the triplet states $|T\rangle$ in the two-site subsystem [36]. In the experimental RF signal we only observe shifts in the amplitude and phase of the resonator response, which always gives a positive relative value.

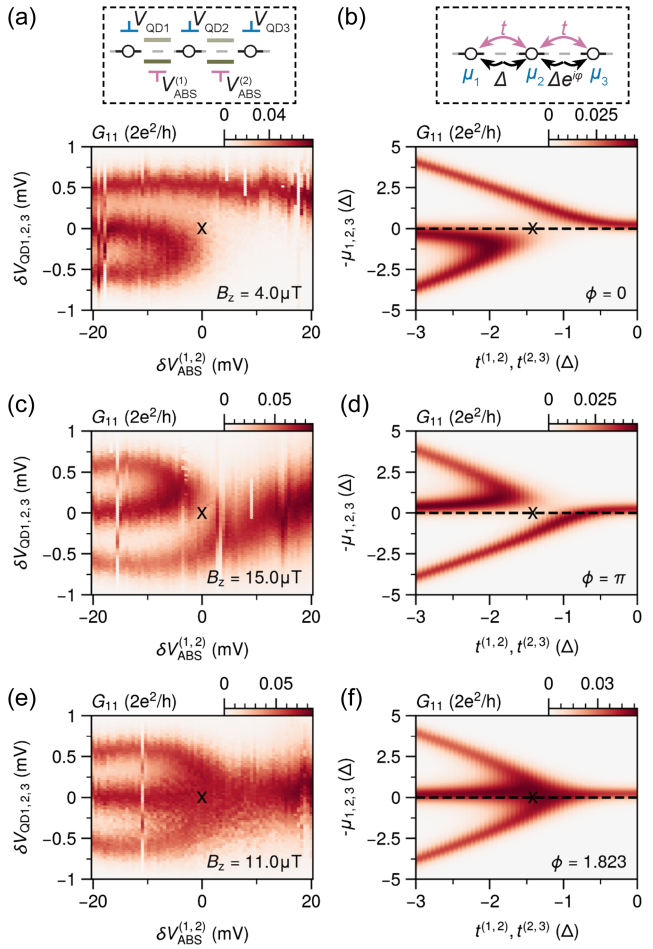


FIG. 4. Superconducting phase as tuning knob. To understand where zero-energy modes arise in the full three-site system, a larger parameter space is explored (procedure detailed in Fig. S8). For each QD pair, sweet spot values are obtained, denoted as $\delta V_{ABS}^{(i)} = 0$. Zero-bias conductance measurements are performed upon simultaneously varying δV_{QDi} versus sweeping $V_{ABS}^{(i)}$ around their sweet-spots. (a) Measurement obtained for $B_z = 4$ μT, corresponding roughly to $\phi = 0$. (b) We compare this to a numerical simulation, where all μ and all t parameters are swept together, for fixed Δ. (c)–(f) We repeat the measurements and simulations for $B_z = 15$ μT (c), corresponding rouhgly to $\phi = \pi$ (d) and (e) $B_z = 11$ μT corresponding to (f) $\phi \approx 1.82$.

contrast to the two-site systems in isolation, which are resilient against local perturbations (Fig. 2), as well as to the behavior observed for three-site systems at finite magnetic fields [17,18]. We find the behavior closely matches the numerical simulations in Fig. 3(b).

Superconducting phase control: We now turn our attention to the final tunable parameter, the superconducting phase difference. With two sites, this phase can be gauged away and therefore does not affect the energy spectra. This is no longer the case when a third site is added [12,23,38,39]. To study the effect of this, we look for ground-state degeneracies in the larger parameter space around the $V_{ABS}^{(1)}$ and $V_{ABS}^{(2)}$ values that corresponded to two-site sweet spots. Sweeping all three QDs around their charge degeneracy points simultaneously and varying both $V_{ABS}^{(1)}$ and $V_{ABS}^{(2)}$, we first map out the conditions that give rise to zero-bias conductance when $\phi = 0$, shown in Fig. 4(a). The "x" marks the point in parameter space where ZBPs arise in the two-site systems in isolation. In accordance with Fig. 3, there is no zero-bias conductance at this point in the three-site system. We compare the measurement to calculated conductance from the effective model, when all μ_i are varied simultaneously versus $t^{(1,2)} = t^{(2,3)}$, for fixed $\Delta^{(1,2)} = \Delta^{(2,3)}$. This does not directly correspond to the experiment, where CAR and ECT are both affected (nonlinearly) by the ABS voltages, but is expected to qualitatively match the data. We find indeed the same degeneracy structure in Fig. 4(b). Next, we apply a small out-of-plane field B_z through the superconducting loop corresponding to a π phase and repeat the measurement [Fig. 4(c)]. Interestingly, this results in a mirrored pattern, matching well with the theory [Fig. 4(d)]. While at π phase we still do not yield a degeneracy at the two-site sweet spot parameters (marked by "x"), the evolution from Fig. 4(a)

implies this should be possible to achieve when fine-tuning the SC phase. Sweeping the phase for the degeneracy to cross $\mu_i = 0$ at $\delta V_{\mathrm{ABS}}^{(1,2)} = 0$, we arrive at the measurement shown in Fig. 4(e). Theoretically, we find this corresponds to the exact phase of $\phi = \arccos(-1/4)$, shown in Fig. 4(f) (see Methods). At this angle, the system in fact exhibits a threefold (strongly) degenerate spectrum at the point $\mu = 0$, $t = \sqrt{2}\Delta$. Going further, we find this point lies along a line in the $\phi - t$ parameter space, parametrized by

$$t^{(i,j)} = \sqrt{-1/2\cos(\varphi)}\Delta^{(i,j)}. \tag{2}$$

For each of these points the systems spectrum is strongly degenerate at $\mu = 0$. We include an expanded discussion of the properties of these strong degeneracies in the End Matter.

Conclusions—We have studied a superconducting extension of the Fermi-Hubbard model in short semiconductor-superconductor hybdrid quantum dot arrays. For both two- and three-site systems, we explore experimentally their parameter space in search of ground-state degeneracies. In the case of two sites, we find close agreement with the predictions put forth in [22], which suggests that a strongly threefold degenerate energy spectrum produces robust Majorana Kramers pairs [30,31] or $\mathbb{Z}_3$ parafermions at sweet spots in parameter space. We identify these configurations through the experimental observation of robust zero-bias conductance peaks in this system. Notably, such excitations can have applications in topological quantum computing [24,40–42], but were typically so far only predicted for more intricate physical platforms [43–51]. Whether our platform, hosting nonlocal many-body Kramers pairs, has potential use in this context remains a subject of further research. Upon extending the system to three sites, we similarly find threefold ground-state degeneracies when sweeping the system's larger parameter space including the superconducting phase. A theoretical analysis shows these to be consistent with strongly degenerate spectra along fine-tuned configurations of the system. In contrast to the two-site system, these degeneracies are never robust against (all) on-site perturbations. We interpret this as being consistent with previous predictions that strong degeneracies in quasi-one-dimensional systems are generally not robust against local perturbations [24,37]. Given the close agreement between theory and experiment, we expect our system to allow for quantum simulation of larger systems beyond computational feasibility. Extending the system to two dimensions, we foresee the platform can be used for studying and understanding strongly correlated phenomena when subjected to superconducting correlations.

Acknowledgments—We thank C. Thomas, D. Xiao and M. J. Manfra for the provision of the 2DEG materials. We thank O. W. B. Benningshof, T. Orton, and J. D. Mensingh for technical assistance with the cryogenic electronics. We thank M. Burrello for his comments on the fractionalized modes and F. Zatelli for valuable input on the manuscript. The research at Delft was supported by the Dutch National Science Foundation (NWO), Microsoft Corporation Station Q, and a grant from Top consortium for Knowledge and Innovation program (TKI). S. G. and M. W. acknowledge financial support from the Horizon Europe Framework Program of the European Commission through the European Innovation Council Pathfinder Grant No. 101115315 (QuKiT). S. M. acknowledges funding from the Dutch Organization for Scientific Research (NWO) through No. OCENW.GROOT.2019.004.

Q. W., I. K., and S. L. D. t. H. fabricated the devices. Y. Z. and I. K. fabricated the resonator circuits. C. G. P. and I. K. designed the measurement setup. Measurements were performed by S. L. D. t. H. Theoretical analysis was performed by S. M., S. L. D. t. H., A. M. B., and M. W. The manuscript was written by S. M., S. L. D. t. H., M. W., and S. G., with input from all coauthors. S. G. supervised the experimental work in Delft.

Data availability—All raw data obtained in relation to this Letter, the code to generate the theoretical results, and the scripts to reproduce the figures from the raw data are available on Zenodo [52].

[1] J. Hubbard and B. H. Flowers, Electron correlations in narrow energy bands, Proc. R. Soc. A **276**, 238 (1963).
[2] D. P. Arovas, E. Berg, S. A. Kivelson, and S. Raghu, The Hubbard model, Annu. Rev. Condens. Matter Phys. **13**, 239 (2022).
[3] P. A. Lee, N. Nagaosa, and X.-G. Wen, Doping a Mott insulator: Physics of high-temperature superconductivity, Rev. Mod. Phys. **78**, 17 (2006).
[4] T. Esslinger, Fermi-Hubbard physics with atoms in an optical lattice, Annu. Rev. Condens. Matter Phys. **1**, 129 (2010).
[5] M. Johanning, A. F. Varón, and C. Wunderlich, Quantum simulations with cold trapped ions, J. Phys. B **42**, 154009 (2009).
[6] S. Schmidt and J. Koch, Circuit QED lattices: Towards quantum simulation with superconducting circuits, Ann. Phys. (Berlin) **525**, 395 (2013).
[7] A. A. Houck, H. E. Türeci, and J. Koch, On-chip quantum simulation with superconducting circuits, Nat. Phys. **8**, 292 (2012).
[8] S. Yang, X. Wang, and S. Das Sarma, Generic Hubbard model description of semiconductor quantum-dot spin qubits, Phys. Rev. B **83**, 161301(R) (2011).
[9] T. Hensgens, T. Fujita, L. Janssen, X. Li, C. J. Van Diepen, C. Reichl, W. Wegscheider, S. Das Sarma, and L. M. K. Vandersypen, Quantum simulation of a Fermi–Hubbard model using a semiconductor quantum dot array, Nature (London) **548**, 70 (2017).

[10] T. Byrnes, N. Y. Kim, K. Kusudo, and Y. Yamamoto, Quantum simulation of Fermi-Hubbard models in semiconductor quantum-dot arrays, Phys. Rev. B **78**, 075320 (2008).
[11] A. Y. Kitaev, Unpaired Majorana fermions in quantum wires, Phys. Usp. **44**, 131 (2001).
[12] J. D. Sau and S. D. Sarma, Realizing a robust practical Majorana chain in a quantum-dot-superconductor linear array, Nat. Commun. **3**, 964 (2012).
[13] M. Leijnse and K. Flensberg, Parity qubits and poor man's Majorana bound states in double quantum dots, Phys. Rev. B **86**, 134528 (2012).
[14] I. C. Fulga, A. Haim, A. R. Akhmerov, and Y. Oreg, Adaptive tuning of Majorana fermions in a quantum dot chain, New J. Phys. **15**, 045020 (2013).
[15] T. Dvir, G. Wang, N. van Loo, C.-X. Liu, G. P. Mazur, A. Bordin, S. L. D. ten Haaf, J.-Y. Wang, D. van Driel, F. Zatelli, X. Li, F. K. Malinowski, S. Gazibegovic, G. Badawy, E. P. A. M. Bakkers, M. Wimmer, and L. P. Kouwenhoven, Realization of a minimal Kitaev chain in coupled quantum dots, Nature (London) **614**, 445 (2023).
[16] S. L. D. ten Haaf, Q. Wang, A. M. Bozkurt, C.-X. Liu, I. Kulesh, P. Kim, D. Xiao, C. Thomas, M. J. Manfra, T. Dvir, M. Wimmer, and S. Goswami, A two-site Kitaev chain in a two-dimensional electron gas, Nature (London) **630**, 329 (2024).
[17] A. Bordin, C.-X. Liu, T. Dvir, F. Zatelli, S. L. D. ten Haaf, D. van Driel, G. Wang, N. van Loo, Y. Zhang, J. C. Wolff, T. Van Caekenberghe, G. Badawy, S. Gazibegovic, E. P. A. M. Bakkers, M. Wimmer, L. P. Kouwenhoven, and G. P. Mazur, Enhanced Majorana stability in a three-site Kitaev chain, Nat. Nanotechnol. **20**, 726 (2025).
[18] S. L. D. ten Haaf, Y. Zhang, Q. Wang, A. Bordin, C.-X. Liu, I. Kulesh, V. P. M. Sietses, C. G. Prosko, D. Xiao, C. Thomas, M. J. Manfra, M. Wimmer, and S. Goswami, Observation of edge and bulk states in a three-site Kitaev chain, Nature (London) **641**, 890 (2025).
[19] C.-X. Liu, G. Wang, T. Dvir, and M. Wimmer, Tunable superconducting coupling of quantum dots via Andreev bound states in semiconductor-superconductor nanowires, Phys. Rev. Lett. **129**, 267701 (2022).
[20] A. Tsintzis, R. S. Souto, and M. Leijnse, Creating and detecting poor man's Majorana bound states in interacting quantum dots, Phys. Rev. B **106**, L201404 (2022).
[21] F. Zatelli, D. van Driel, D. Xu, G. Wang, C.-X. Liu, A. Bordin, B. Roovers, G. P. Mazur, N. van Loo, J. C. Wolff, A. M. Bozkurt, G. Badawy, S. Gazibegovic, E. P. A. M. Bakkers, M. Wimmer, L. P. Kouwenhoven, and T. Dvir, Robust poor man's Majorana zero modes using Yu-Shiba-Rusinov states, Nat. Commun. **15**, 7933 (2024).
[22] A. M. Bozkurt, S. Miles, S. L. D. ten Haaf, C.-X. Liu, F. Hassler, and M. Wimmer, Interaction-induced strong zero modes in short quantum dot chains with time-reversal symmetry, SciPost Phys. **18**, 206 (2025).
[23] P. Fendley, Parafermionic edge zero modes in Z_n-invariant spin chains, J. Stat. Mech. (2012) P11020.
[24] J. Alicea and P. Fendley, Topological phases with parafermions: Theory and blueprints, Annu. Rev. Condens. Matter Phys. **7**, 119 (2016).
[25] G. Wang, T. Dvir, G. P. Mazur, C.-X. Liu, N. van Loo, S. L. D. ten Haaf, A. Bordin, S. Gazibegovic, G. Badawy, E. P. A. M. Bakkers, M. Wimmer, and L. P. Kouwenhoven, Singlet and triplet Cooper pair splitting in hybrid superconducting nanowires, Nature (London) **612**, 448 (2022).
[26] A. Bordin, X. Li, D. van Driel, J. C. Wolff, Q. Wang, S. L. D. ten Haaf, G. Wang, N. van Loo, L. P. Kouwenhoven, and T. Dvir, Crossed Andreev reflection and elastic cotunneling in three quantum dots coupled by superconductors, Phys. Rev. Lett. **132**, 056602 (2024).
[27] A. Bordin, G. Wang, C.-X. Liu, S. L. D. ten Haaf, N. van Loo, G. P. Mazur, D. Xu, D. van Driel, F. Zatelli, S. Gazibegovic, G. Badawy, E. P. A. M. Bakkers, M. Wimmer, L. P. Kouwenhoven, and T. Dvir, Tunable crossed Andreev reflection and elastic cotunneling in hybrid nanowires, Phys. Rev. X **13**, 031031 (2023).
[28] Q. Wang, S. L. D. ten Haaf, I. Kulesh, D. Xiao, C. Thomas, M. J. Manfra, and S. Goswami, Triplet correlations in Cooper pair splitters realized in a two-dimensional electron gas, Nat. Commun. **14**, 4876 (2023).
[29] See Supplemental Material at http://link.aps.org/supplemental/10.1103/nz6v-xxrv for data and details about experimental and numerical methods.
[30] T. E. O'Brien, A. R. Wright, and M. Veldhorst, Many-particle majorana bound states: Derivation and signatures in superconducting double quantum dots, Phys. Status Solidi (b) **252**, 1731 (2015).
[31] A. R. Wright and M. Veldhorst, Localized many-particle majorana modes with vanishing time-reversal symmetry breaking in double quantum dots, Phys. Rev. Lett. **111**, 096801 (2013).
[32] D. Reilly, C. Marcus, M. Hanson, and A. Gossard, Fast single-charge sensing with a RF quantum point contact, Appl. Phys. Lett. **91**, 162101 (2007).
[33] M. Jung, M. Schroer, K. Petersson, and J. R. Petta, Radio frequency charge sensing in InAs nanowire double quantum dots, Appl. Phys. Lett. **100**, 253508 (2012).
[34] D. Razmadze, D. Sabonis, F. K. Malinowski, G. C. Ménard, S. Pauka, H. Nguyen, D. M. van Zanten, and E. C. O'Farrell, J. Suter, P. Krogstrup, F. Kuemmeth, and C. M. Marcus, Radio-frequency methods for Majorana-based quantum devices: Fast charge sensing and phase-diagram mapping, Phys. Rev. Appl. **11**, 064011 (2019).
[35] I. Kulesh, S. L. D. ten Haaf, Q. Wang, Vincent P. M. Sietses, Y. Zhang, S. R. Roelofs, C. G. Prosko, D. Xiao, C. Thomas, M. J. Manfra, and S. Goswami, Flux-controlled two-site Kitaev chain, Phys. Rev. Lett. **135**, 056301 (2025).
[36] Z. Scherübl, A. Pályi, and S. Csonka, Transport signatures of an Andreev molecule in a quantum dot–superconductor–quantum dot setup, Beilstein J. Nanotechnol. **10**, 363 (2019).
[37] A. S. Jermyn, Roger S. K. Mong, J. Alicea, and P. Fendley, Stability of zero modes in parafermion chains, Phys. Rev. B **90**, 165106 (2014).
[38] S. Howes, L. P. Kadanoff, and M. Den Nijs, Quantum model for commensurate-incommensurate transitions, Nucl. Phys. **B215**, 169 (1983).
[39] S. Ostlund, Incommensurate and commensurate phases in asymmetric clock models, Phys. Rev. B **24**, 398 (1981).
[40] P. Gao, Y.-P. He, and X.-J. Liu, Symmetry-protected non-Abelian braiding of Majorana Kramers pairs, Phys. Rev. B **94**, 224509 (2016).
[41] C. Schrade and L. Fu, Quantum computing with Majorana Kramers pairs, Phys. Rev. Lett. **129**, 227002 (2022).

[42] H. Pan, J. Jia, and Z. Qiao, Fusion rules for Majorana Kramers pairs in time-reversal invariant topological superconductors, Phys. Rev. B **111**, 115414 (2025).
[43] Chris L. M. Wong and K. T. Law, Majorana kramers doublets in $d_{x^2-y^2}$-wave superconductors with Rashba spin-orbit coupling, Phys. Rev. B **86**, 184516 (2012).
[44] F. Zhang, C. L. Kane, and E. J. Mele, Time-reversal-invariant topological superconductivity and Majorana Kramers pairs, Phys. Rev. Lett. **111**, 056402 (2013).
[45] A. Keselman, L. Fu, A. Stern, and E. Berg, Inducing time-reversal-invariant topological superconductivity and fermion parity pumping in quantum wires, Phys. Rev. Lett. **111**, 116402 (2013).
[46] J. Klinovaja and D. Loss, Time-reversal invariant parafermions in interacting Rashba nanowires, Phys. Rev. B **90**, 045118 (2014).
[47] J. Klinovaja, A. Yacoby, and D. Loss, Kramers pairs of Majorana fermions and parafermions in fractional topological insulators, Phys. Rev. B **90**, 155447 (2014).
[48] A. Haim, A. Keselman, E. Berg, and Y. Oreg, Time-reversal-invariant topological superconductivity induced by repulsive interactions in quantum wires, Phys. Rev. B **89**, 220504 (R) (2014).
[49] X.-J. Liu, Chris L. M. Wong, and K. T. Law, Non-abelian Majorana doublets in time-reversal-invariant topological superconductors, Phys. Rev. X **4**, 021018 (2014).
[50] C. Schrade, A. A. Zyuzin, J. Klinovaja, and D. Loss, Proximity-induced π Josephson junctions in topological insulators and Kramers pairs of Majorana fermions, Phys. Rev. Lett. **115**, 237001 (2015).
[51] M. Thakurathi, P. Simon, I. Mandal, J. Klinovaja, and D. Loss, Majorana Kramers pairs in Rashba double nanowires with interactions and disorder, Phys. Rev. B **97**, 045415 (2018).
[52] S. L. D. ten Haaf and S. Miles, Data and Code for "Probing ground-state degeneracies of a strongly interacting Fermi-Hubbard model with superconducting correlations" (2025), 10.5281/zenodo.17872114.
[53] R. L. R. C. Teixeira and L. G. G. V. Dias da Silva, Edge $\mathbb{z}_3$ parafermions in fermionic lattices, Phys. Rev. B **105**, 195121 (2022).
[54] I. A. Day, S. Miles, H. K. Kerstens, D. Varjas, and A. R. Akhmerov, Codebase release 2.1 for Pymablock, SciPost Phys. Codebases 50 (2025).

End Matter

Strong degeneracies through control over the superconducting phase—In Fig. 4 we have observed that tuning the superconducting phase difference yields configurations for which the degeneracy lines cross $\mu_i == 0$. When $t^{(i,j)} = \sqrt{2}\Delta^{(i,j)} =$ (the two-site sweet spot), the phase at which this crossing occurs is $\phi = \arccos(-1/4)$, where the entire spectrum is found to be strongly degenerate. We find that by allowing $\Delta^{(i,j)} \neq \sqrt{2}t^{(i,j)}$, there exists a whole line in parameter space for which the spectrum is strongly, threefold degenerate. Fixing $\mu_i = 0$ and calculating the spectrum analytically (see Methods), we obtain the condition for degeneracy to be

$$t^{(i,j)} = \sqrt{-\frac{1}{2\cos(\varphi)}}\Delta^{(i,j)}, \tag{A1}$$

where $\Delta^{(1,2)} = \Delta^{(2,3)}$ and $t^{(1,2)} = t^{(2,3)}$. Along this line [Fig. 5(a)], the Hamiltonian in Eq. (1) commutes with both the fermion parity operator $P_F = \prod_{i,\sigma}(1 - 2n_{i,\sigma})$, and a $\mathbb{Z}_3$-parity operator $P_3 = \exp[i(2\pi/3)\sum_i(n_{i,\uparrow} + 2n_{i,\downarrow})]$ [53]. The emergence of this commutator relation can be understood from the point of chirality [24]. The 27 levels contained in the low-energy subspace split into seven distinct manifolds: three triply degenerate levels with $E < 0$, 1 nine-fold degenerate manifold at $E = 0$, and another three triply degenerate manifold with $E > 0$ (see Methods). Ideally, a point can be found where the strongly degenerate spectrum again gives rise to Majorana Kramers Pairs or $\mathbb{Z}_3$ parafermions, as obtained for the two-site system in Ref. [22]. To assess this, we numerically calculate the linear derivatives of the energy splitting between odd and even ground states with respect to the individual dot chemical potentials, $\partial_{\mu_i}(E_{\text{even},0} - E_{\text{odd},0})$ [Fig. 5(b)]. Doing so for all φ, we find that the ground state degeneracy is unaffected by changes of the chemical potential of the central dot, μ_2, in linear order. In contrast, the degeneracy splits linearly when varying the chemical potential of the outer dots, μ_1, μ_3, except for two points where the coupling in linear order of perturbation theory vanishes. Numerically these phases are found to be at $\varphi^* \in \{1.86, 4.42\}$ (cf. Fig. 5). To verify this, we numerically calculate a perturbative expansion for the ground state manifold when perturbed by any $\mu_i(n_{i\uparrow} + n_{i\downarrow})$ [54], i.e., local perturbations to the chemical potential of one of the QDs. Since the perturbations neither break parity nor time-reversal symmetry, we can understand the system's response by considering the ratio $\delta E_{\text{even}}/\delta E_{\text{odd}}$ of the energy shifts $E_i \to E_i^{(0)} + \delta E_i$ induced within each parity sector. To linear order in μ_i, we indeed recover the spectral insensitivity to changes as $\delta E_{\text{even}}(\mu_i) = \delta E_{\text{odd}}(\mu_i)$ at φ_i^*. Expanding to second order in μ_i, we however find that the splitting at φ_i^* differs and therefore breaks the degeneracy [Fig. 5(e)]. Consequently, we will not be able to find Majorana Kramers pairs or $\mathbb{Z}_3$-parafermion operators that are robust against local perturbations as previously [22] for two sites. We note that this is in line with previous conclusions for strong degeneracies in chiral spin chains [23]. To conclude, we consider the conductance signatures at two points along the triply degenerate line [Figs. 5(c) and 5(d)]. While the perturbative results suggest a splitting of the levels with

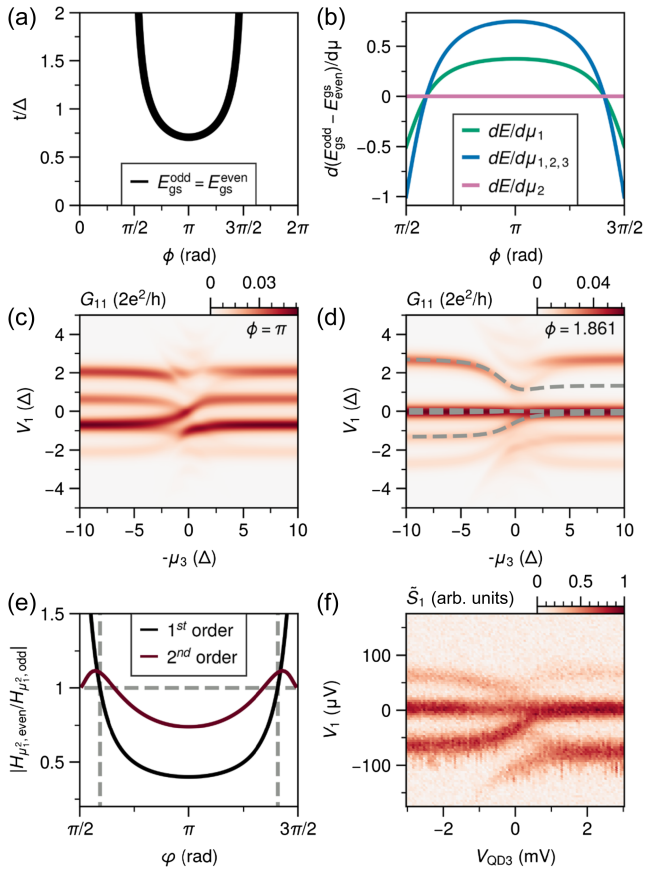


FIG. 5. Strongly degenerate ground states in the three-site chain. (a) Analytical solution yielding $E_{gs}^{odd} = E_{gs}^{even}$ for the three-site chain when $\mu_i = 0$ [given by Eq. (A1)], resulting in a strongly degenerate spectrum. (b) Derivative of the energy difference between the odd and even ground states with respect to detuning μ. The derivatives vanish at two specific points. The significance can be seen when comparing the conductance spectrum of detuning μ_3 at (c) $\phi = \pi$ and (d) $\phi = 1.861$. The numerical energy spectrum is overlaid in (d) to highlight that a small energy splitting still arises at larger detuning of μ_3. (e) Perturbative expansion of first order and second order derivatives, highlighting that the higher order derivative does not vanish at the same ϕ value as the first order. (f) Measurement of $\tilde{S}_1$ when detuning QDR, with the settings in Fig. 4(c), in order to compare with the predicted spectrum (d). Repeated measurements for a range of B_x values is shown in Fig. S9 [29].

the chemical potential, we find in conductance that this splitting can become very small and not possible to resolve due to broadening from temperature effects. Experimentally, we indeed observe that a phase value can be found where a seemingly robust zero-bias conductance peak appears [Fig. 5(f)]. We want to highlight that this behavior is not to be generally expected, but only along this fine-tuned line of parameters.